ESMO GOOD SCIENCE BETTER MEDICINE BEST PRACTICE

Annals of Oncology 30: 1521–1530, 2019
doi:10.1093/annonc/mdz207
Published online 8 July 2019

ORIGINAL ARTICLE

Suppressed immune microenvironment and repertoire in brain metastases from patients with resected non-small-cell lung cancer

Y. Kudo[1,2], C. Haymaker[1], J. Zhang[3], A. Reuben[4], D. Y. Duose[1], J. Fujimoto[1], S. Roy-Chowdhuri[5], L. M. Solis Soto[1], H. Dejima[1], E. R. Parra[1], B. Mino[1], R. Abraham[1], N. Ikeda[2], A. Vaporcyan[6], D. Gibbons[4], J. Zhang[4], F. F. Lang[7], R. Luthra[1,8], J. J. Lee[3], C. Moran[5], J. T. Huse[1,5], H. Kadara[1] & I. I. Wistuba[1,4*]

[1]Department of Translational Molecular Pathology, The University of Texas MD Anderson Cancer Center, Houston, USA; [2]Department of Surgery, Tokyo Medical University, Tokyo, Japan; Departments of [3]Biostatistics; [4]Thoracic/Head and Neck Medical Oncology; [5]Pathology; [6]Thoracic and Cardiovascular Surgery; [7]Neurosurgery; [8]Hematopathology, The University of Texas MD Anderson Cancer Center, Houston, USA

Correspondence to: Dr Ignacio I. Wistuba, Department of Translational Molecular Pathology, University of Texas MD Anderson Cancer Center, 2130 Holcombe Blvd., Houston, TX 77030, USA. Tel: +1-713-792-9866; Fax: +1-713-834-6082; E-mail: iiwistuba@mdanderson.org

Background: The tumor immune microenvironment (TIME) of lung cancer brain metastasis is largely unexplored. We carried out immune profiling and sequencing analysis of paired resected primary tumors and brain metastases of non-small-cell lung carcinoma (NSCLC).

Patients and methods: TIME profiling of archival formalin-fixed and paraffin-embedded specimens of paired primary tumors and brain metastases from 39 patients with surgically resected NSCLCs was carried out using a 770 immune gene expression panel and by T-cell receptor beta repertoire (TCRβ) sequencing. Immunohistochemistry was carried out for validation. Targeted sequencing was carried out to catalog hot spot mutations in cancer genes.

Results: Somatic hot spot mutations were mostly shared between both tumor sites (28/39 patients; 71%). We identified 161 differentially expressed genes, indicating inhibition of dendritic cell maturation, Th1, and leukocyte extravasation signaling pathways, in brain metastases compared with primary tumors ($P < 0.01$). The proinflammatory cell adhesion molecule vascular cell adhesion protein 1 was significantly suppressed in brain metastases compared with primary tumors. Brain metastases exhibited lower T cell and elevated macrophage infiltration compared with primary tumors ($P < 0.001$). T-cell clones were expanded in 64% of brain metastases compared with their corresponding primary tumors. Furthermore, while TCR repertoires were largely shared between paired brain metastases and primary tumors, T-cell densities were sparse in the metastases.

Conclusion: We present findings that suggest that the TIME in brain metastases from NSCLC is immunosuppressed and comprises immune phenotypes (e.g. immunosuppressive tumor-associated macrophages) that may help guide immunotherapeutic strategies for NSCLC brain metastases.

Key words: tumor microenvironment, non-small-cell lung cancer, brain metastases, VCAM1, TCR repertoire, tumor-associated macrophage

Introduction

Brain metastases are common in advanced lung cancer patients and a major cause of mortality [1]. Additionally, 10% of patients who receive surgical resection for early-stage (e.g. resectable) non-small-cell lung cancer (NSCLC) are found to exhibit recurrence in the form of brain metastasis [2, 3]. The median survival of patients with untreated NSCLC brain metastases is a mere 1–2 months [4]. The primary therapeutic strategy for brain metastases includes surgery, stereotactic radiosurgery, and whole brain radiation therapy, with these therapies bestowing minimal

survival advantages [5]. Driver mutated genes, such as epidermal growth factor receptor (*EGFR*) mutation or an anaplastic lymphoma kinase rearrangements, are commonly used to guide personalized targeted therapies for primary NSCLC, but with relatively far more limited success for brain metastases [6, 7].

Evasion of the host immune response is a hallmark of cancer progression. Inhibition of cancer immunosuppression, e.g. by targeting immune checkpoints, has provided opportune strategies for immunotherapy of patients with advanced stage cancers such as NSCLC and melanoma [8, 9]. Markers for response to immune checkpoint inhibition include relatively high tumor mutation burdens, elevated expression of immune checkpoints such as tumoral programed cell death ligand 1 (PD-L1) and a 'hot' or inflamed state characterized by tumor-infiltrating lymphocytes (TILs) [10]. In contrast to primary NSCLCs, features of the tumor immune microenvironment (TIME) in corresponding brain metastases are far less characterized, in part due to the difficulty in obtaining brain metastases biopsies.

Here, we carried out immune profiling and sequencing of matched pairs of archival formalin-fixed and paraffin-embedded (FFPE) primary lung tumors and brain metastases from 39 patients with resected NSCLC. While brain metastases and primary tumors display mostly similar driver hot spot mutation profiles, we find that the TIME of brain metastases is, overall, more immunosuppressed than that of primary NSCLCs. We also show that T-cell clonal density and richness is lower in brain metastases compared with primary lung tumors.

Methods

NSCLC cohort

One hundred and fourteen matched FFPE archival non-malignant lung parenchymas adjacent to tumors ($n = 36$), primary lung tumors ($n = 39$) and brain metastases ($n = 39$) were obtained from 39 NSCLC patients who underwent surgical resection for both primary lung cancer and brain metastases at The University of Texas MD Anderson Cancer Center under approved institutional review board protocols. Patients who received neoadjuvant chemotherapy were excluded from the study. The characteristics of the 39 patients are summarized in Table 1. This cohort comprised 24 adenocarcinomas, 8 squamous cell carcinomas, 4 large cell neuroendocrine carcinomas and 4 other histologies. The major recurrent pattern of brain metastases was metachronous ($n = 37$ patients). Thirty-six brain metastases cases received glucocorticoid treatment before surgical resection. Seven cases received radiotherapy for brain metastases before surgical resection.

DNA/RNA extraction

Hematoxylin and eosin stained sections of surgical specimens were reviewed by an experienced pathologist. Five to fifteen 10 μm-thickness unstained slides from FFPE tissues were deparaffinized, and then macrodissection was carried out to extract RNA and DNA from tumor tissues using AllPrep DNA/RNA FFPE kit (from Qiagen).

Targeted DNA sequencing analysis

Targeted sequencing of extracted DNA was carried out with the Ion AmpliSeq Cancer Hotspot Panel version 2 (CHPv2) on the Ion S5XL platform (ThermoFisher Scientific, Waltham, MA). Custom-developed, in-house software (OncoSeek) was utilized to interface the data with the Integrative Genome Viewer, to filter repeat errors due to nucleotide homopolymer regions, to compare replicate samples and to annotate the sequencing variants [11].

Gene expression analysis by nCounter platform and functional pathways analysis

Gene expression analysis was carried out using nCounter PanCancer Immune Profiling Panel (NanoString Technologies, Seattle, WA). To identify differentially expressed genes (DEGs), a two sample *t*-test was carried out. Bonferroni method was applied for multiple-testing adjustment to generate adjusted *P*-values with an $\alpha < 0.001$ used as the statistical threshold. After identifying DEGs, Ingenuity Pathways Analysis (Qiagen) was used to functionally organize the genes into modulated pathways and topological gene–gene interaction networks. In addition, immune cell profiling was carried out using the entire gene sets on nSolver 4.0 (NanoString Technologies).

Immunohistochemistry analysis

Five-micrometer tissue sections were prepared from available FFPE blocks of primary NSCLCs and matched brain metastases, and then mounted on to slides for immunohistochemistry (IHC) staining. All slides were stained with antibodies raised against CD8 (clone C8/144B, 1 : 25, ThermoFisher Scientific) and against vascular cell adhesion protein 1 (VCAM1) (clone EPR5047, 1 : 500, Abcam). Brain metastases specimens were also stained with antibodies against CD68 (clone PG-M1, 1 : 450, Dako) and TMEM119 (1 : 100, Abcam). Quantification of immunoreactivity was carried out by selecting 5×1 mm^2 regions within the tumor followed by enumerating average densities as number of positive cells per millimeter square for CD8 and percentage of positive areas for VCAM1 using the Aperio Image Toolbox analysis software (Leica Microsystems). The evaluation of microglia and macrophages in the brain metastases was carried out by assessing CD68 and TMEM119 immunoreactivity. CD68+TMEM119+ denoted microglial cells, whereas CD68+TMEM119− staining denoted monocyte-derived macrophages.

TCR*β* sequencing analysis

TCRβ complementarity-determining region 3 sequencing was carried out using the ImmunoSEQ Assay pipeline (Adaptive Biotechnologies, Seattle, WA). Clonality was defined as '1—normalized entropy'; normalized entropy was calculated by summing the frequency of each clone times the log (base 2) of the same frequency over all productive reads in a sample. Richness was defined as the number of unique nucleotide rearrangements in a sample. Differential abundance tool on the ImmunoSEQ Analyzer was used to assess T-cell clone frequencies and abundances. Any clones with cumulative abundance of <10 were disregarded in the differential abundance comparison. Only clones with an adjusted *P*-value <0.01 were identified as expanded clones. Shared clones were defined as those detected in both samples with 10 or more cumulative abundance.

Statistical analysis

Non-parametric Mann–Whitney *U* tests were carried out when comparing values of their gene expression level or number of immune cells among lung primary tumors, non-malignant lung parenchyma and brain metastases. All *P*-values were two-sided, and *P*-values of <0.05 denoted statistical significance. All statistical analysis was carried out in R version 3.3.0.

Detailed methods are described in supplementary Tables S1 and S2, available at *Annals of Oncology* online.

Table 1. Patient's characteristics ($n = 39$)

Variable	Category	Number
Sex	Male	17
	Female	22
Age at operation for brain metastases	Median (range)	61 (40–84) years old
Smoking habits	Smoker	35
	Never smoker	4
Histology	Adenocarcinoma	24
	Squamous cell carcinoma	8
	Large cell neuroendocrine carcinoma	3
	Others	4
Pathological tumor size of lung cancer	Median (range)	3.2 (0.7–13.0) cm
Pathological stage (TNM 7th edition)	I	14
	II	12
	III	10
	IV	3
Adjuvant chemotherapy	Present	20
Type of brain metastasis	Synchronous	2
	Metachronous	37
Interval between operation for lung cancer and operation for brain metastases	Median (range)	481 (−2607 to 1933) days
Radiological size of brain metastases	Median (range)	3.1 (1.0–7.0) cm
Number of brain metastases before the operation	1	29
	2	5
	3	2
	4 or more	3
Radiation therapy for brain metastasis before the neurosurgery	Present (interval between radiotherapy and the neurosurgery)	7 (2 months–1 year and 3 months)

Others: three non-small-cell lung carcinomas no-otherwise specified (NOS) and one adenosquamous cell carcinoma.

Results

High concordance of detected mutations between primary lung tumors and brain metastases

We examined the 78 paired tumor samples by targeted DNA sequencing for hot spot mutations. The samples comprised 158 somatic mutations, which included 127 single nucleotide variants (SNVs) and 31 insertions or deletions (indels). The primary lung cancers and the brain metastases comprised 76 and 82 mutations, respectively. The most frequent mutations resided in *TP53*, *KRAS*, and *EGFR* genes (Figure 1A). When we compared mutations among paired cases, the detected variants were shared in 28 patients (71%), and 6 patients (15%) had partially shared mutations (Figure 1B). Furthermore, variant allelic frequencies (VAFs) of each shared mutation were increased in brain metastases compared with the paired primary lung tumor (Figure 1C). Out of 72 shared mutations, VAFs were increased in 60 mutations and the median difference in the VAFs was 21.6% (range 1.6%–63.4%).

Immune suppressive microenvironment in brain metastases

To evaluate gene expression signatures of infiltrating immune cells, we analyzed immune gene expression profiles in the 78 paired brain metastases and primary lung tumors using the nCounter PanCancer Immune Profiling Panel. We first identified 161 DEGs between the brain metastases and the primary lung tumor using an adjusted *P*-value cutoff of <0.001. Clustering analysis revealed that the identified gene were able to distinguish, for the most part, brain metastases from primary NSCLCs (Figure 2A). Functional pathways analysis revealed various significantly modulated pathways including inhibition (indicated by negative *z*-scores) of dendritic cell (DC) maturation (−1.604), Th1 immune response (−1.633) and leukocyte extravasation signaling (−1.508). The DEGs also embodied activation (indicated by positive z-score) of toll-like receptor signaling (2.828) in the brain metastases, compared with the lung tumors (Figure 2B). We then carried out topological gene–gene interaction network analysis. We noted that the top network analysis comprised markedly suppressed expression ($P < 0.001$) of the adhesion molecule VCAM1 and that comprised highly inter-connected network gene neighbors (Figure 2C). Furthermore, reduced expression of VCAM1 at the protein level in the brain metastases was validated by IHC analysis (Figure 2D). These results suggest that antigen presentation, e.g. by DCs, as well as extravasation of lymphocytes and adhesion of leukocytes (reduced VCAM1) are suppressed in brain metastases compared with matched primary NSCLCs. though antigen exposure using toll-like receptors were observed.

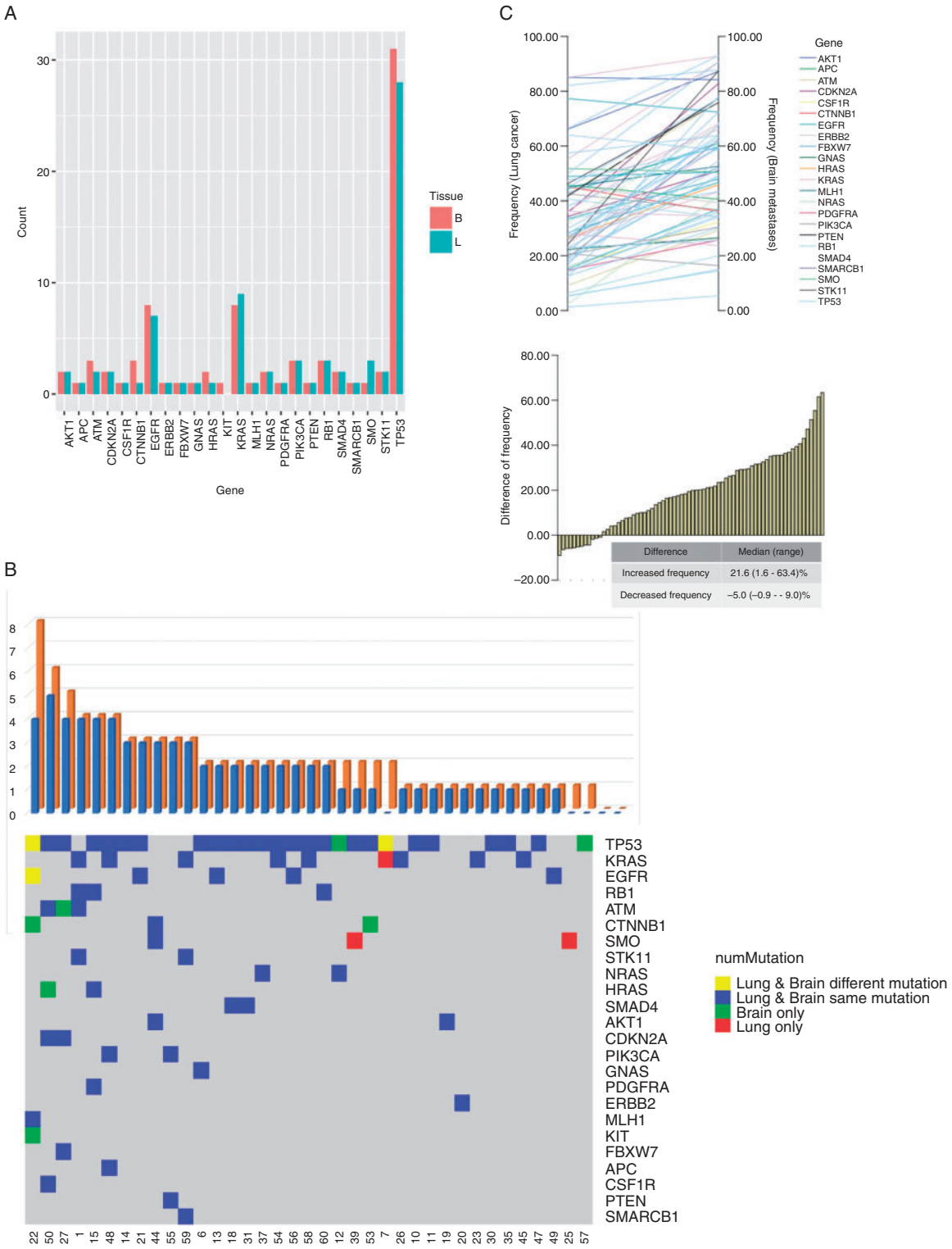

Figure 1. Targeted sequence analysis of hot spot mutations in matched primary lung tumors and brain metastases. (A) Relationship between detected mutations and frequency in primary lung cancer (*L*) and brain metastases (*B*). *Y*-axis represented number of each detected mutations. (B) Shared mutation across primary lung tumors and brain metastases. Top bar graph depicts the number of detected mutations (*Y*-axis) in each sample (*X*-axis). The orange bar represents total number of detected mutations and the blue bar represents shared mutations between primary lung tumors and brain metastases. The lower heat map denotes the identified hot spot mutations in primary lung tumors and brain metastases. Rows represents variants and columns denote samples. Patterns of sharing of variants between brain metastases and matched primary lung tumors are denoted by the color as indicated in the figure legend on the right. (C) Variant allele frequencies (VAFs) of the identified 72 variants that are shared between the primary lung tumors (left scale) and brain metastases (right scale). Different types of mutations are denoted by the indicated colors. The right bar graph showed difference of allelic frequency in shared mutations.

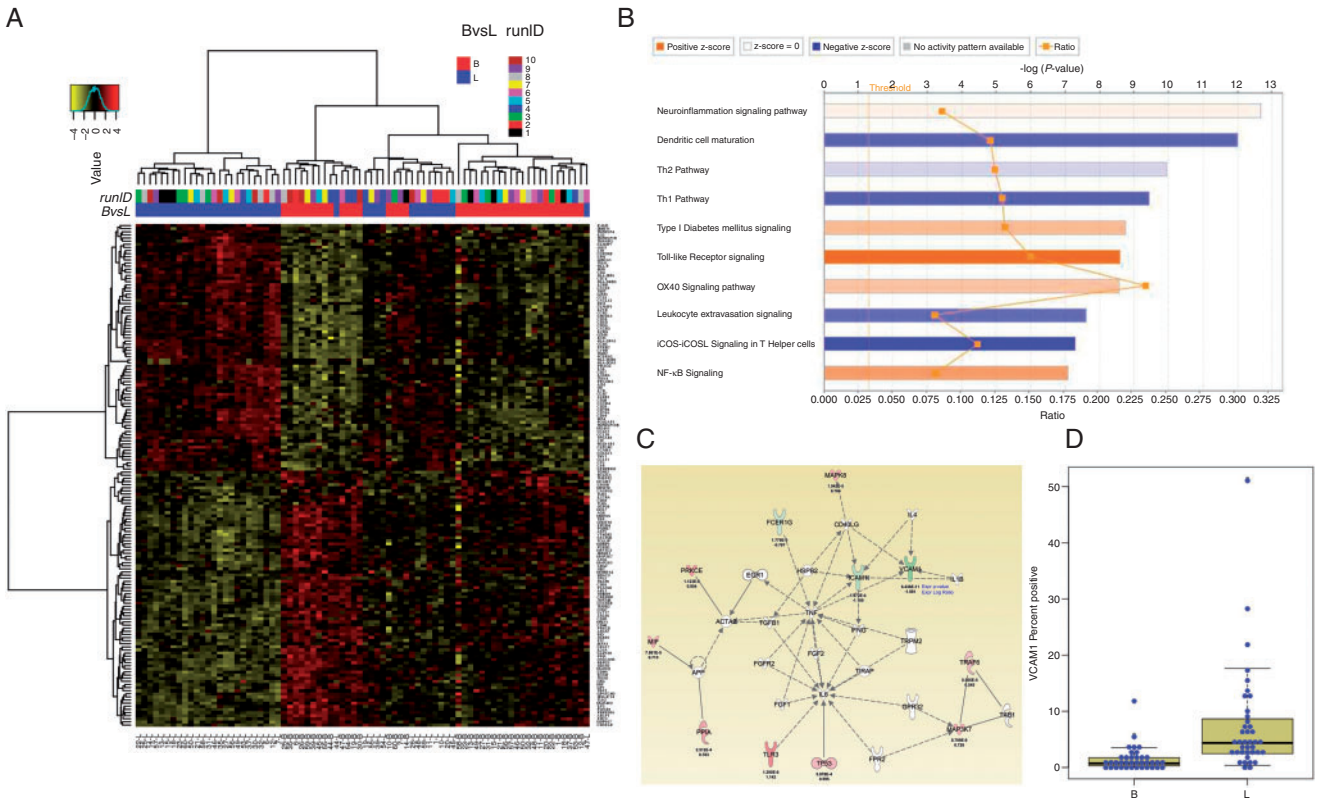

Figure 2. Immune gene expression profiling of matched primary lung tumors and brain metastases. (A) Differentially expressed immune-associated genes (n=161) were identified as described in the Methods section and are depicted in the heat map. Rows denote that genes and columns represent samples (relatively up-regulated, yellow; down-regulated, blue). Tissue types are represented in the accompanying legend (brain metastases, B; primary lung tumor, L). (B) Functional pathways analysis of the differentially expressed genes was carried out using the commercially available software Ingenuity Pathways Analysis. The top ten pathways, sorted by statistical significance (−log base 10 of P-values), are shown. (C) Topological gene–gene interaction network Top network analysis by using 161 differentially expressed genes (DEGs) on Ingenuity Pathway Analysis. Red and green color indicated up-regulated and down-regulated genes in brain metastases, respectively. (D) Immunohistochemistry of VCAM1 protein was carried out as described in the Methods section. Percentage of areas with positive VCAM1 expression against total area between brain metastases (*B*) and primary lung tumors (*L*).

We then questioned the impact of glucocorticoid treatment on immune gene expression profiles in the brain metastases. We found no significant DEGs in brain metastases between patients with and without glucocorticoid treatment before the metastasis resection (supplementary Figure S1, available at *Annals of Oncology* online). We also found that immune-related gene expression profiles did not correlate with NSCLC patients' outcome (data not shown). Furthermore, differences in number of immune cell subpopulations, estimated based on the differential immune gene profiles, were not statistically significantly between patients with and without glucocorticoid treatment (supplementary Figure S2, available at *Annals of Oncology* online).

Low TILs and high fraction of macrophages in brain metastases

We then computed relative abundances of immune cell subpopulations based on expression counts from the entire panel of surveyed genes. The abundance measurements of Th1 or CD8 T genes were significant lower in brain metastases than in the primary tumors ($P<0.001$) (Figure 3A). In addition, TILs were significantly lower in the brain metastases than the lung tumors ($P<0.001$) (Figure 3B). Moreover, we found statistically significantly reduced levels of CD8+ T cells in brain metastases by IHC analysis (Figure 3C). Also, the relative abundances of DC and macrophage genes were significantly lower in brain metastases compared with primary lung tumors ($P<0.001$ and $P=0.013$, respectively) (Figure 3A). Ratios of macrophage to TIL genes were statistically significantly higher in the brain metastases ($P<0.001$) (Figure 3B). Gene expression levels of the macrophage (M2-like) marker arginase-I (*ARG1*) were statistically higher in the brain metastases compared with lung tumors ($P<0.001$) (supplementary Figure S3, available at *Annals of Oncology* online). Since gene expression profiling does not allow for an accurate discrimination between peripherally derived macrophages and brain resident microglia, the expression of TMEM119 (microglia marker) was assessed using IHC. This analysis revealed that the majority of CD68+ immune cells in the brain metastases were negative for TMEM119 and, thus, represented macrophages (94% of patients assessed; supplementary Figure S4, available at *Annals of Oncology* online). Overall, these data demonstrate that brain metastases compared with primary

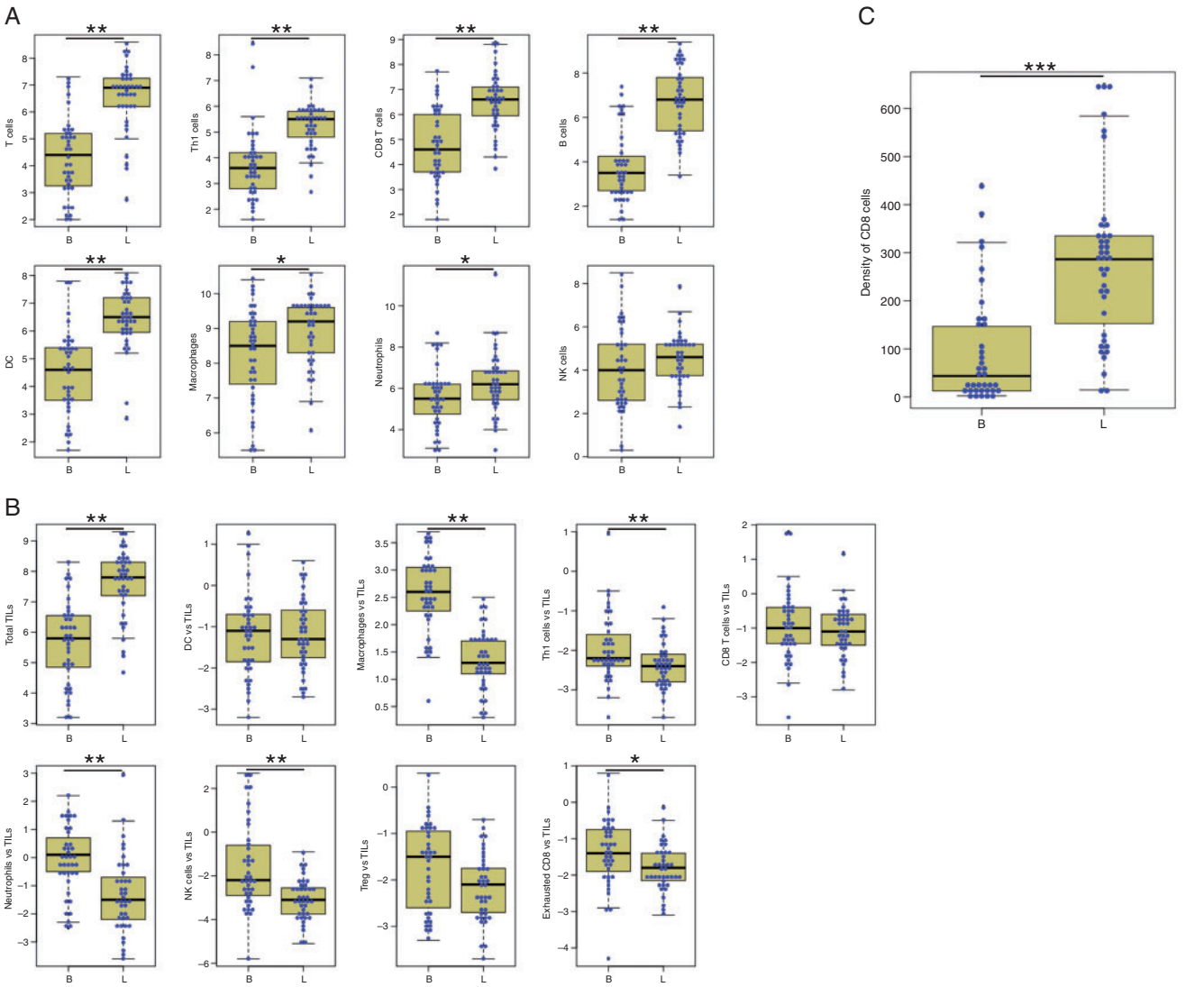

Figure 3. Increased macrophages and reduced TILs in brain metastases relative to primary lung tumors. (A) Computational assessment of immune subpopulations based on gene expression analysis was carried out as described in the Methods section. Abundance measurements of T cells, Th1 cells, CD8 T cells, B cells, dendritic cells (DC), macrophages, neutrophils, and NK cells in brain metastases (*B*) and primary lung tumors (*L*). $^{**}P<0.01$; $^{*}P<0.05$. (B) Abundance measurements of TILs and ratio of each immune cell subpopulation against TILs in brain metastases (*B*) and primary lung tumors (*L*). The assessed immune subpopulations included DCs, macrophages, Th1 cells, CD8 T cells, neutrophils, NK cells, regulatory T cells (Treg), and exhausted CD8 cells. $^{**}P<0.01$, $^{*}P<0.05$. (C) Density of CD8 cells in brain metastases (*B*) and primary lung tumors (*L*). $^{***}P<0.001$.

lung tumors display reduced T cells, including Th1 cells or TILs, as well as elevated monocyte-derived macrophages suggestive of immunosuppression in the metastatic sites.

Low density and richness of T cells, but high frequency of shared T-cell clones in brain metastases

To comparatively characterize T-cell repertoires in brain metastases and primary lung tumors, we conducted TCRβ sequencing of 39 paired brain metastases and primary lung tumors as well as 36 matched non-malignant lung parenchyma. We found no statistically significant differences in clonality among the three types of tissues ($P=0.922$) (Figure 4A). T-cell richness was significantly lower in the brain metastases compared with the primary lung tumors or the non-malignant lung parenchyma (Figure 4A). Similarly, T-cell densities were also statistically significantly lower in brain metastases.

Next, we focused on majority of T-cell clones that were associated with specific antigens after exposure in each tissue. Figure 4B depicts representative distribution of clones that resided in the brain metastases and/or the paired lung tumors; we excluded any clones with <10 of cumulative abundance from further analysis. Surprisingly, most clones in the brain metastases were shared with paired lung tumors with the median ratio of the shared clones at 100% (Figure 4C). We subsequently analyzed significantly expanded clones in the brain metastases. We found that the clones in brain metastases were expanded in 25 patients

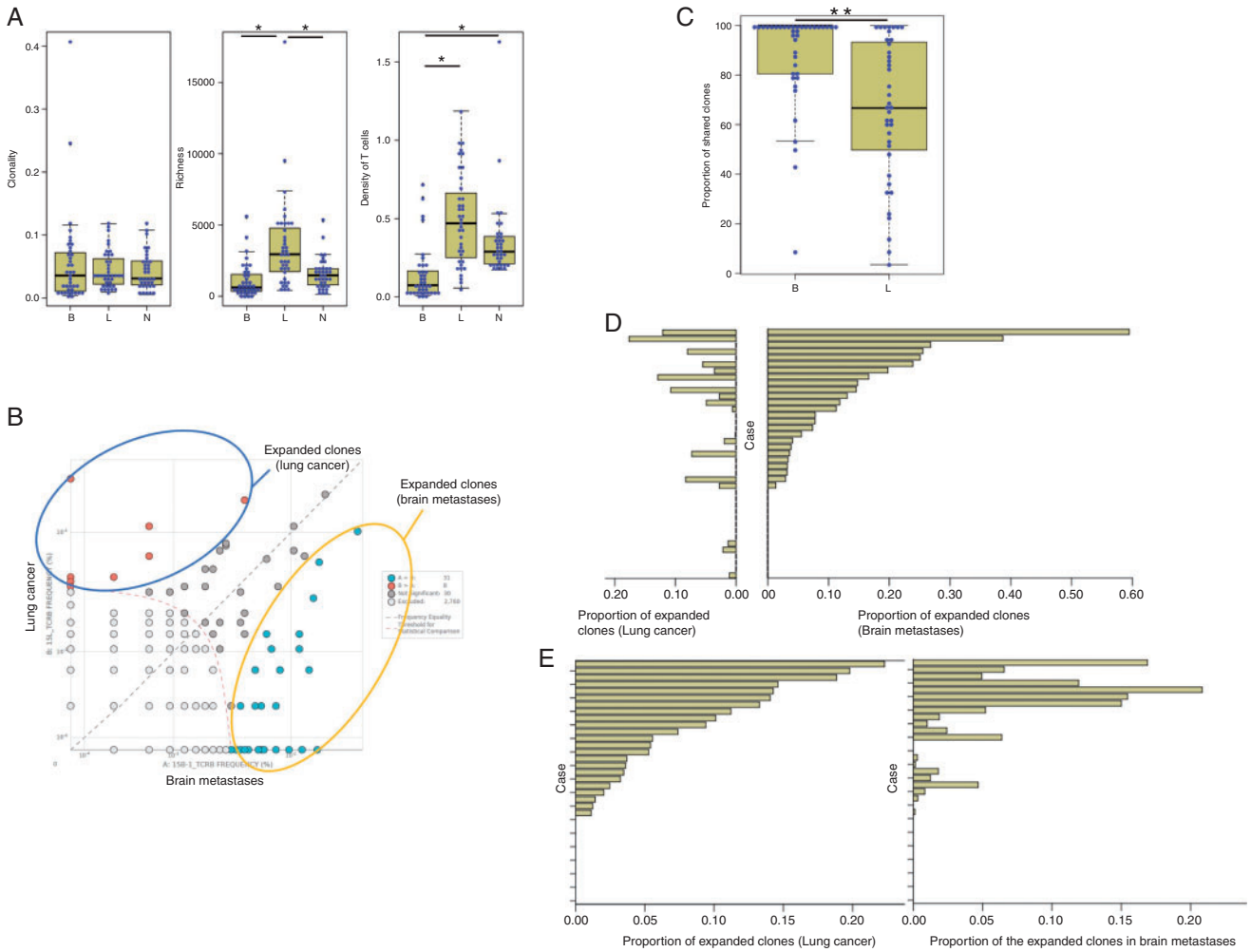

Figure 4. Attenuated T-cell density and richness in brain metastases compared with matched primary lung tumors. (A) TCRβ sequencing of brain metastases and matched primary lung tumors was carried out as described in the Methods section and in supplementary data, available at *Annals of Oncology* online. Clonality, richness, and density of T cells in brain metastases (B), primary lung tumors (L) and uninvolved normal lung parenchyma (N). (B) Representative distribution of T-cell clones residing in either brain metastases and/or paired primary lung tumors. Clones with <10 of cumulative abundance under the threshold are shown in light gray dots. The blue dots represent differentially abundant clones in brain metastases, which were expanded clones ($P<0.01$). The red dots denote differentially abundant clones in primary lung tumors, which were expanded clones ($P<0.01$). The dark gray dots showed clones with no significant difference in abundance. (C) Proportion of shared T-cell clones between brain metastases (*B*) and primary lung tumors (*L*). **$P<0.001$. (D) Frequency of expanded clones in brain metastases and in primary lung tumors. The frequencies denote proportions of expanded clones of the total clones. (E) Left bar graph depicts frequency of expanded clones in primary lung tumors against paired non-malignant lung parenchyma. The right bar graph depicts frequency of expanded clones from the 23 cases paired brain metastases.

(64%), and the median frequency of expanded clones against total clones in those patients was 11.2% (Figure 4D). Likewise, T-cell clones were statistically significantly expanded in 23 patients of the primary lung tumor (63%), and the median frequency of expanded cloned against total clones was 5.6% in the 23 patients with expanded clones (Figure 4E). Furthermore, those expanded clones were detected in 20 patients of the brain metastases (87%) while the median frequency of the shared clones was 1.8% (Figure 4E). The data also suggested that tumor-related antigens were shared between the brain metastases and the lung tumors in most cases and that clonal expansion occurred in the brain metastases whereas T cells were not infiltrated sufficiently. Of interest, TCRβ sequencing analysis did not show significant difference in clonality, richness, and density of T cells in brain metastasis sites between those patients who received and did not receive glucocorticoid treatment prior surgical resection (supplementary Figure S5, available at *Annals of Oncology* online). These findings, in accordance with our immune gene expression profiling analyses above, suggest a state of reduced T-cell migration and augmented immunosuppression in the brain metastases relative to primary lung tumors.

Discussion

Here we interrogated matched primary NSCLCs and brain metastases by sequencing and immune profiling. This effect is exemplified by (i) inhibition of pathways implicating leukocyte

extravasation, DC maturation, and Th1 immune responses; (ii) suppressed expression of molecules (e.g. VCAM1) that promote leukocyte adhesion to inflammatory sites; (iii) increased expression of markers implicating protumorigenic M2-like macrophages; (iv) reduced CD8+ T cell and TIL infiltration and (v) reduced T-cell richness and density demonstrated by TCR sequencing. These differential immune effects were observed in spite of the high proportions of shared tumoral driver hot spot mutations and T-cell clones between both compartments. Our study suggests that the tumor immune microenvironment in brain metastases compared with primary lung tumors is further immunosuppressed and suggests avenues for devising new strategies for immunotherapy of brain metastases—e.g. by targeting immunosuppressive macrophages.

The brain has been considered as an immune privileged organ, however, this concept is being revised as a lymphatic vessel network of brain tissues was reported in the dura mater in mice [12–14]. Our coupled immune gene expression profiling, pathways analysis, and topological gene–gene network survey showed an immune suppressive environment in the brain metastases, in part exemplified by inhibition of DC maturation, low frequency of CD8+ T cells and Th1 cells as well as reduced lymphocyte extravasation and leukocyte adhesion. In the brain microenvironment, microglia represent first line innate immunity and play crucial roles as antigen presenting cells [15]. Once activated, these cells produce proinflammatory cytokines, chemokines and upregulate immunomodulatory surface markers; subsequently, these immune responses allow immune cells or modulators to penetrate brain tissues through the blood brain barrier [16]. Several reports have found that bone marrow-derived monocytes are recruited to brain tumors, where they differentiate into monocyte-derived macrophages [17–19]. In this context, our finding that the microglial marker TMEM119 was mostly absent in brain metastases suggests that the majority of macrophages present in these lesions were derived from peripheral monocytes and not from microglias. It is important to note that we had found that brain metastases compared with primary lung tumors exhibited elevated expression of *ARG1*, an enzyme in L-arginine metabolism thought to be a marker of anti-inflammatory and protumorigenic M2-like macrophages [20]. Thus, it is reasonable to suggest that tumor-associate macrophages (TAMs) may also exert immunosuppressive roles in the immune microenvironment of brain metastases. Our immune gene expression profiling and pathways analyses are also in line with previous reports demonstrating reduced TILs in brain metastases compared with matched primary tumors of lung and breast cancer patients [21, 22]. Accordingly, we also observed markedly suppressed expression of VCAM1, a molecule that plays crucial roles in mediating the adhesion of various leukocytes [16]. It is plausible that VCAM1 suppression is casually linked to the observed reduced T-cell infiltration in the brain metastases. Supporting this supposition are reports showing that drugs that interrupt the binding of α4 integrin to VCAM1 are effective in treating diseases involving uncontrollable/elevated infiltration of lymphocytes into inflammatory sites [23, 24].

Our findings on an increased TAM phenotype in brain metastases suggest that targeting immunosuppressive TAMs may be a viable immunotherapeutic approach for clinical management of brain metastases in resected NSCLC. A CSF-1R inhibitor, which targets TAMs, has shown promise in melanoma and augmented chemotherapeutic responses [25]. Additionally, earlier work has shown that strategies targeting promoters of TAM recruitment such as CCL2 [26, 27] and CXCL12/CXCR4 [28, 29] attenuated breast and prostate cancer metastasis. Furthermore, agents targeting activators of M2-macrophage reprograming such as STAT3 inhibited immunosuppressive cytokine profiles of myeloid-derived suppressor cells [30]. Caetano et al. have shown that the cytokine IL-6 promotes immunosuppressive profiles in lung adenocarcinoma in part by M2 polarization of macrophages [31]. In the same study, antibodies against IL-6 inhibited lung adenocarcinoma development concomitant with an M2 to M1 shift in macrophage polarization [31]. Of note, clinical trials are underway to assess the immunotherapeutic potential of targeting CSF1/CSF1R, CCL2/CCR2, and IL6R in various solid tumors including bone metastasis [25]. Future work and clinical studies are warranted to examine the immunotherapeutic potential of agents targeting immunosuppressive properties and cytokine profiles of TAMs in the clinical management of brain metastases in NSCLC.

Concomitant with our immune gene expression profiling analyses is our finding by TCR sequencing that T-cell richness and densities, as well as TILs, were reduced in the immune microenvironment of brain metastases, despite that TCR repertoires were, for the most part, shared with matched primary NSCLCs. It is conceivable that most tumor antigens are shared between primary lung tumors and brain metastases. It is worthwhile to mention that a recent study demonstrated that clonal overlap of entire TCR sequences was limited between the primary lung cancers and brain metastases displaying a 0.23 Morisita overlap index [22]. In contrast to our study design, the study by Mansfield et al. [22] did not focus on analysis of abundant T-cell clones, i.e. those with accentuated roles in the immune microenvironment. It is noteworthy that we found that somatic hot spot mutations were, for the most part, shared between primary lung tumor and matched brain metastases. Yet, for some of these variants their VAFs were increased in the brain metastases suggestive of clonal expansion. It is not clear how these variants may disparately interplay with the host immune response across both compartments. Future studies are warranted to discern the landscape of tumoral mutations in brain metastases and how they relate to the immunosuppressive microenvironment.

Our study is not without limitations. It is not clear how our findings on the immune microenvironment of brain metastases in NSCLC patients are specific to primary lung malignancy. Also it is not discerned how the immune microenvironment of brain metastases compares to that of primary brain tumors. Previous studies have shown that the majority of immune cells within primary brain tumors are macrophages and often comprise up to 30% of the tumor mass [32–34]. Of note, Wang et al. demonstrated that there are increased type-2 (M2) polarized macrophages in mesenchymal gliomas [35]. Furthermore, earlier work demonstrated that for some brain tumors, the macrophages within/surrounding the tumor are bone marrow derived (rather than microglial) [19], which is line with what we observed in brain metastases from patients with primary NSCLC. It is plausible that there are common immune microenvironment features between

both brain metastases and primary brain tumors and, thus, there may be immunotherapeutic strategies (e.g. targeting TAMs) that may be applicable to both of brain metastases from NSCLC and primary brain tumors. It is noteworthy we employed targeted mutational hot spot profiling to primarily interrogate the spectrum of canonical driver SNVs. For the most part, this strategy captured truncal variants and not subclonal mutations that may have been favorably selected in the transition of primary NSCLCs to brain metastasis—though we noted increased VAFs for some of these truncal variants suggestive of clonal selection/expansion from the primary NSCLCs to brain metastases. Of note, we found, following histopathological evaluation, that tumor cellularity was significantly ($P < 0.01$, of the paired Wilcoxon rank sum test) elevated in the brain metastatic lesions compared with matched primary lung tumors in the NSCLC patients (supplementary Figure S6, available at *Annals of Oncology* online) which may explain, in part, the increased VAFs for the various SNVs in the brain metastases. Future studies employing whole-genome or single-cell approaches coupled with immune profiling are warranted to study the landscape of genotype–immune phenotype interactions in brain metastases of NSCLC patients. Another limitation of our study is that the majority (36 out of 39) of patients received glucocorticoid treatment before metastasis surgical resection. Patients with brain metastases commonly exhibit brain edema or neurological symptoms and most receive glucocorticoid therapy before neurosurgery [1, 5, 36]. Glucocorticoids are reported to elicit inhibitory immune responses via reduced secretion of inflammatory cytokines and leukocyte trafficking [37]. Nonetheless, our comparative immune profiling and sequencing analysis of cases with and without glucocorticoid treatment demonstrated similar overall host immune responses/microenvironments in brain metastases between both groups. Future studies are warranted to fully elucidate the impact of glucocorticoid treatment on the interplay between the host immune response and brain metastases as well as on responses to immunotherapeutic regimens.

In conclusion, we demonstrate, by comparative immune gene profiling and sequencing analyses, that the immune microenvironment of brain metastases is overall immunosuppressed, in part by increased infiltration of TAMs, when compared with matched primary tumors in NSCLC patients. Our study provides new insights into the interplay between the host immune response and brain metastases in NSCLC patients and paves the way for developing new immunotherapeutic strategies, e.g. by targeting TAMs and their immunosuppressive profiles/properties, for lung cancer patients with distant spread to the brain.

Funding

This study was supported in part by a Cancer Prevention Research Institute of Texas Multi-Investigator Research Award (grant number RP160668), The University of Texas Lung Specialized Programs of Research Excellence grant (grant number P50CA70907 to IIW], and MD Anderson's Institutional Tissue Bank Award through the Cancer Center Support Grant (grant number P30CA016672) from the National Cancer Institute.

Disclosure

The authors have declared no conflicts of interest.

References

1. Dawe DE, Greenspoon JN, Ellis PM. Brain metastases in non-small-cell lung cancer. Clin Lung Cancer 2014; 15(4): 249–257.
2. Barnholtz-Sloan JS, Sloan AE, Davis FG et al. Incidence proportions of brain metastases in patients diagnosed (1973 to 2001) in the Metropolitan Detroit Cancer Surveillance System. J Clin Oncol 2004; 22(14): 2865–2872.
3. Hubbs JL, Boyd JA, Hollis D et al. Factors associated with the development of brain metastases: analysis of 975 patients with early stage non-small cell lung cancer. Cancer 2010; 116(21): 5038–5046.
4. Markesbery WR, Brooks WH, Gupta GD, Young AB. Treatment for patients with cerebral metastases. Arch Neurol 1978; 35(11): 754–756.
5. Ricciardi S, de Marinis F. Multimodality management of non-small cell lung cancer patients with brain metastases. Curr Opin Oncol 2010; 22(2): 86–93.
6. Soria JC, Ohe Y, Vansteenkiste J et al. Osimertinib in untreated EGFR-mutated advanced non-small-cell lung cancer. N Engl J Med 2018; 378(2): 113–125.
7. Peters S, Camidge DR, Shaw AT et al. Alectinib versus crizotinib in untreated ALK-positive non-small-cell lung cancer. N Engl J Med 2017; 377: 829–838.
8. Goldberg SB, Gettinger SN, Mahajan A et al. Pembrolizumab for patients with melanoma or non-small-cell lung cancer and untreated brain metastases: early analysis of a non-randomised, open-label, phase 2 trial. Lancet Oncol 2016; 17: 976–983.
9. Tawbi HA, Forsyth PA, Algazi A et al. Combined nivolumab and ipilimumab in melanoma metastatic to the brain. N Engl J Med 2018; 379(8): 722–730.
10. Mazzaschi G, Madeddu D, Falco A et al. Low PD-1 expression in cytotoxic CD8(+) tumor-infiltrating lymphocytes confers an immune-privileged tissue microenvironment in NSCLC with a prognostic and predictive value. Clin Cancer Res 2018; 24(2): 407–419.
11. Singh RR, Patel KP, Routbort MJ et al. Clinical validation of a next-generation sequencing screen for mutational hotspots in 46 cancer-related genes. J Mol Diagn 2013; 15(5): 607–622.
12. Louveau A, Smirnov I, Keyes TJ et al. Structural and functional features of central nervous system lymphatic vessels. Nature 2015; 523(7560): 337–341.
13. Aspelund A, Antila S, Proulx ST et al. A dural lymphatic vascular system that drains brain interstitial fluid and macromolecules. J Exp Med 2015; 212(7): 991–999.
14. Louveau A, Harris TH, Kipnis J. Revisiting the mechanisms of CNS immune privilege. Trends Immunol 2015; 36(10): 569–577.
15. Lehnardt S. Innate immunity and neuroinflammation in the CNS: the role of microglia in Toll-like receptor-mediated neuronal injury. Glia 2010; 58(3): 253–263.
16. Wilson EH, Weninger W, Hunter CA. Trafficking of immune cells in the central nervous system. J Clin Invest 2010; 120(5): 1368–1379.
17. Shi C, Pamer EG. Monocyte recruitment during infection and inflammation. Nat Rev Immunol 2011; 11(11): 762–774.
18. Bowman RL, Klemm F, Akkari L et al. Macrophage ontogeny underlies differences in tumor-specific education in brain malignancies. Cell Rep 2016; 17(9): 2445–2459.
19. Chen Z, Feng X, Herting CJ et al. Cellular and molecular identity of tumor-associated macrophages in glioblastoma. Cancer Res 2017; 77(9): 2266–2278.
20. Genard G, Lucas S, Michiels C. Reprogramming of tumor-associated macrophages with anticancer therapies: radiotherapy versus chemo- and immunotherapies. Front Immunol 2017; 8: 828.
21. Ogiya R, Niikura N, Kumaki N et al. Comparison of immune microenvironments between primary tumors and brain metastases in patients with breast cancer. Oncotarget 2017; 8(61): 103671–103681.

22. Mansfield AS, Ren H, Sutor S et al. Contraction of T cell richness in lung cancer brain metastases. Sci Rep 2018; 8(1): 2171.
23. Polman CH, O'Connor PW, Havrdova E et al. A randomized, placebo-controlled trial of natalizumab for relapsing multiple sclerosis. N Engl J Med 2006; 354(9): 899–910.
24. Ghosh S, Goldin E, Gordon FH et al. Natalizumab for active Crohn's disease. N Engl J Med 2003; 348(1): 24–32.
25. Poh AR, Ernst M. Targeting macrophages in cancer: from bench to bedside. Front Oncol 2018; 8: 49.
26. Qian BZ, Li J, Zhang H et al. CCL2 recruits inflammatory monocytes to facilitate breast-tumour metastasis. Nature 2011; 475(7355): 222–225.
27. Zhang J, Patel L, Pienta KJ. CC chemokine ligand 2 (CCL2) promotes prostate cancer tumorigenesis and metastasis. Cytokine Growth Factor Rev 2010; 21(1): 41–48.
28. Wong D, Kandagatla P, Korz W, Chinni SR. Targeting CXCR4 with CTCE-9908 inhibits prostate tumor metastasis. BMC Urol 2014; 14: 12.
29. Huang EH, Singh B, Cristofanilli M et al. A CXCR4 antagonist CTCE-9908 inhibits primary tumor growth and metastasis of breast cancer. J Surg Res 2009; 155(2): 231–236.
30. Xin H, Zhang C, Herrmann A et al. Sunitinib inhibition of Stat3 induces renal cell carcinoma tumor cell apoptosis and reduces immunosuppressive cells. Cancer Res 2009; 69(6): 2506–2513.
31. Caetano MS, Zhang H, Cumpian AM et al. IL6 blockade reprograms the lung tumor microenvironment to limit the development and progression of K-ras-mutant lung cancer. Cancer Res 2016; 76(11): 3189–3199.
32. Graeber MB, Scheithauer BW, Kreutzberg GW. Microglia in brain tumors. Glia 2002; 40(2): 252–259.
33. Charles NA, Holland EC, Gilbertson R et al. The brain tumor microenvironment. Glia 2012; 60(3): 502–514.
34. Quail DF, Joyce JA. The microenvironmental landscape of brain tumors. Cancer Cell 2017; 31(3): 326–341.
35. Wang Q, Hu B, Hu X et al. Tumor evolution of glioma-intrinsic gene expression subtypes associates with immunological changes in the microenvironment. Cancer Cell 2017; 32(1): 42–56 e46.
36. Ewend MG, Morris DE, Carey LA et al. Guidelines for the initial management of metastatic brain tumors: role of surgery, radiosurgery, and radiation therapy. J Natl Compr Canc Netw 2008; 6(5): 505–513; quiz 514.
37. Fauci AS, Dale DC, Balow JE. Glucocorticosteroid therapy: mechanisms of action and clinical considerations. Ann Intern Med 1976; 84(3): 304–315.